# Interaction of a free burning arc with regenerative protective layers



Journal of Physics: Conference Series **550** (2014) 012010 doi:10.1088/1742-6596/550/1/012010

# Interaction of a free burning arc with regenerative protective layers

**D Uhrlandt, S Gorchakov, V Brueser, St Franke, A Khakpour, M Lisnyak, R Methling and Th Schoenemann**

Leibniz Institute for Plasma Science and Technology (INP Greifswald), Germany

E-mail: uhrlandt@inp-greifswald.de

**Abstract.** The possible use of protective layers made of ceramic powders for walls in thermal plasma applications is studied. A stable free burning arc of currents up to 5 kA between copper-tungsten electrodes is used to analyse the arc interaction with samples coated by mixtures of $CaCO_3$, $MgCO_3$, and $Mg(OH)_2$ with plaster. By means of optical emission spectroscopy the maximum arc temperature and the radiation impact on the surfaces are estimated to be around 15000 K and 20 $MWm^{-2}$, respectively. Thermographic measurements confirm the efficient protection of substrates by all layer materials. Layers containing $CaCO_3$ lead to the lowest heating of ceramic samples which may be caused by a strong evaporation of the layer material.

## 1. Introduction

The interaction of the arc with electrodes or other walls is the key issue of operation and lifetime of the devices in many applications of thermal plasmas. The arc can be close to chamber walls where the impact by heat and radiation leads to erosion. On the one hand, this erosion can finally damage the chamber and limit the lifetime. On the other hand, the processes of wall erosion can be also beneficial and are used as a main mechanism for pressure build-up and arc extinction in self-blast circuit breakers, for example. In any case, the erosion of electrodes and other walls leads to a modification of the gas properties and therefore has often strong influence on arc ignition and the properties of the established arc. There is a large number of studies of the contact erosion and wall ablation in switching devices due to a dominant role of these processes for the functionality. Most studies are focussed on the impact on dielectric recovery (e.g. in high-current circuit breakers with ablation dominated arcs - see e.g. [1, 2]) or on arc motion and extinction (e.g. in low-voltage circuit breakers with magnetically blown arcs - see e.g. [3, 4, 5]). Progress has been made in particular in the understanding and modelling of the arc interaction and ablation of polytetrafluoroethylene (PTFE) nozzle walls [6]. Here, simple relations of arc energy and arc radiation to the ablation rate are known. Gas-producing polymeric materials as replacements for PTFE are also intensively studied [1, 4, 5].

The unintentional and often crucial erosion of isolating walls has been studied mainly for low-voltage circuit breakers. Here, arc interaction with polymeric materials as well as ceramics and their impact on breaking capacity have been investigated. Less attention has been paid up to know to possibilities of a wall protection with coatings together with a fundamental study of their erosion processes.

This paper describes first steps for an experimental study of such protective layers and their capability to reduce heat impact on walls and erosion. Ideal coatings should have a high robustness and adhesion at the surface and should be cheap and easy to coat. In this study ceramic powder layers of 2 mm thickness are considered which have the additional advantage of cooling during heat impact and self-regeneration after the arc impact. The three substances $CaCO_3$, $MgCO_3$, and $Mg(OH)_2$ are used which build up oxides of $CO_2$ or $H_2O$ due to thermal separation. Under appropriate conditions, for example in a closed chamber, the opposite reactions of the oxides back to carbonates or hydroxides are possible. Hence, over longer times after arc impact the carbonates or hydroxides can be deposited back on the surfaces, and a partly regeneration of the layers can be reached. $Mg(OH)_2$ has the additional advantage to be a fire suppressant medium because of the dissociation to MgO and $H_2O$. A comparison of the behaviour of the three substances is also motivated by the differences of their melting points and thermal conductivity.

First aim of the work is the evaluation of an appropriate setup to study the interaction of the coatings with high-current arcs under reproducible conditions. In contrast to other works, the focus is on the arc impact, the vaporisation and the final thermal impact on the coated wall and not on the changes of the gas medium and its resulting dielectric strength. A free burning arc experiment is considered which allows for optical investigations. High-speed images, spectroscopy of the arc and surface temperature measurements should reveal the different behaviour of the three coatings and indicate the potential protective functionality.

The electrical setup, the substrate properties and the observation methods are given in section 2. The analysis of the arc by optical emission spectroscopy is presented in section 3. Results of thermographic studies of the behaviour of substrates with different coatings after arc interaction are given and discussed in section 4. Section 5 gives final conclusions and an outlook on the next steps.

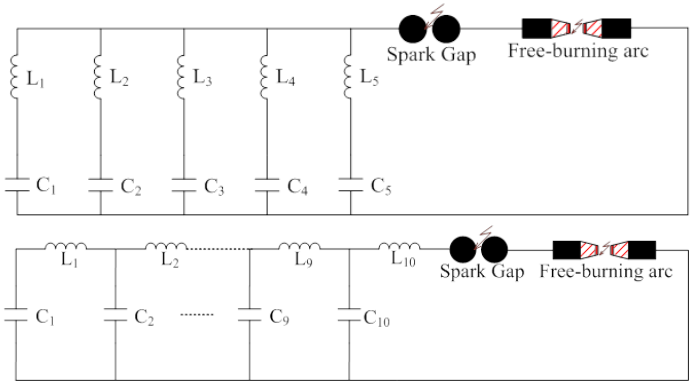


**Figure 1.** Electrical circuit arrangements for a sinusoidal current at 50 Hz (upper part) and for rectangular current pulses (lower part).

## 2. Experimental setup and materials

*Electrical setup* Two options of arc operation have been used for the test of arc interaction with coated substrates. Beside a sinusoidal current at 50 Hz a specific pulsed current generator is used to provide rectangular pulses with peak currents up to 5 kA over 5 ms. The electrical circuits for both arrangements are given in Figure 1. For the sinusoidal current LC elements with $C_1$ to $C_5$=525 $\mu$F and $L_1$ to $L_5$=4700 $\mu$H are coupled in parallel. LC elements with constant capacity $C_1$ to $C_10$= 262.5 $\mu$F and stepwise decreasing inductances from $L_1$=610 $\mu$H, $L_2$=380 $\mu$H, down to $L_9$=260 $\mu$H and $L_{10}$=180 $\mu$H are coupled in series to produce the rectangular pulses. A spark

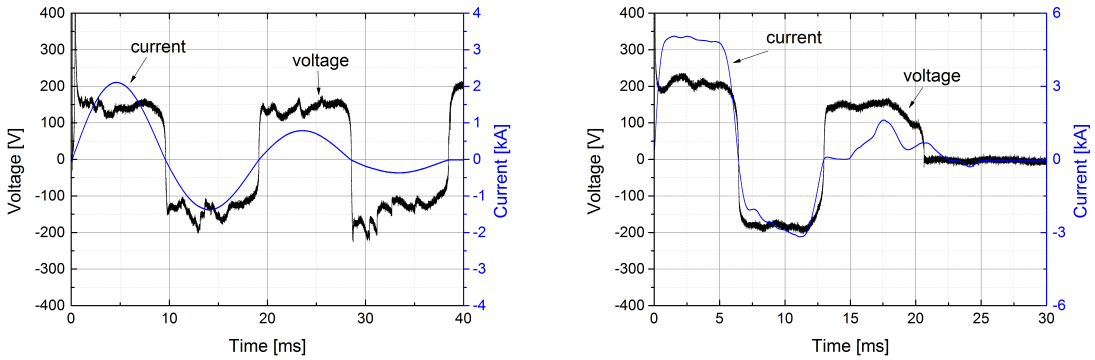


**Figure 2.** Typical current and voltage courses of the AC operation at 50 Hz (left side) and for the rectangular pulses of 5 ms duration (right side).

gap is used as the switch. The current is measured near to the arc gap by a current probe (Pearson monitor). Rectangular pulses are considered to ensure constant arc impact over time as far as possible. Typical waveforms are given in Figure 2. The current amplitude is damped, so that four half waves or pulses of decreasing peak current are measured.

The arc is operated between copper-tungsten rod electrodes of 10 mm diameter in a distance of about 50 mm in ambient air. Ceramic nozzles are used to insulate the sides of the rod electrodes and to ensure a flat and limited arc attachment area. The electrode erosion at current densities larger than $10^8$ $Am^{-2}$ promotes an almost stable arc operation at least near the electrodes by the establishment of copper vapour jets (see [7] for comparison). However, the interaction of these jets from cathode and anode can cause instabilities. The electrode setup is shown in Figure 3. The arc is ignited by a thin copper wire between the electrodes. High-speed videos confirm a vaporisation of the wire in a time period of up to 1 ms. Therefore, the pulse is considered to be nearly unaffected by the wire ignition.

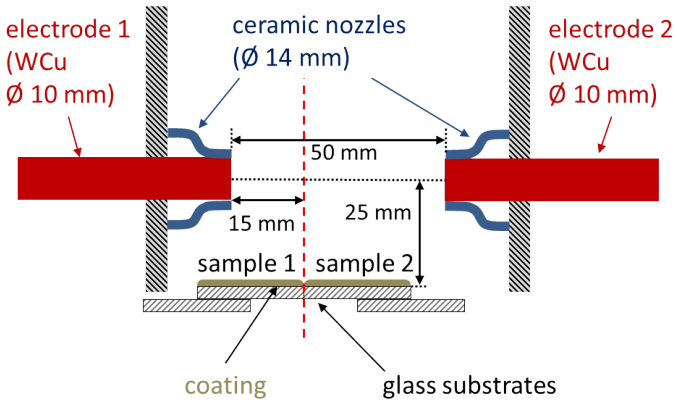


**Figure 3.** Setup of the arc experiment (top view).

*Layer materials and samples* Glass substrates of 3 mm thickness and ceramic substrates of 1 mm thickness are coated with powder layers of approximately 2 mm thickness. Plaster ($Ca[SO_4]\cdot 2H_2O$) has been used as a simple binding agent. Hence, the layers consist of mixtures of the three substances $CaCO_3$, $MgCO_3$, and $Mg(OH)_2$ with plaster (approximately 30%). The

**Figure 4.** Glass substrate with a $CaCO_3$ layer (side and front view).

coating with plaster is rather fragile and not very robust. Experiments have been done also with organic binders. It turned out, that all coatings show strong evaporation during arc interaction which may be dominated by the binder material. For a better comparability of the behaviour of the powder material with respect to evaporation and cooling of the substrates, the binding with plaster has been favoured. The arc interaction with a pure plaster layer has been considered for comparison. Figure 4 shows an example of a glass substrate with a $CaCO_3$ layer.

The substrates are positioned sideward to the arc in distances of 25 mm from the arc axis (electrode 1) as illustrated in Figure 3. Two samples are tested in one pulse in parallel. Because of the axial variation of the arc properties the contact point of the two samples is considered as a reference position in axial direction. This position is marked by a dashed vertical line in both Figures 3 and 5. Only small variations of the arc radiation in the vicinity of this line are expected. Hence, areas on both samples near to the line can be considered as comparable impact zones. Nevertheless, experiments are always repeated with changed positions of the samples.

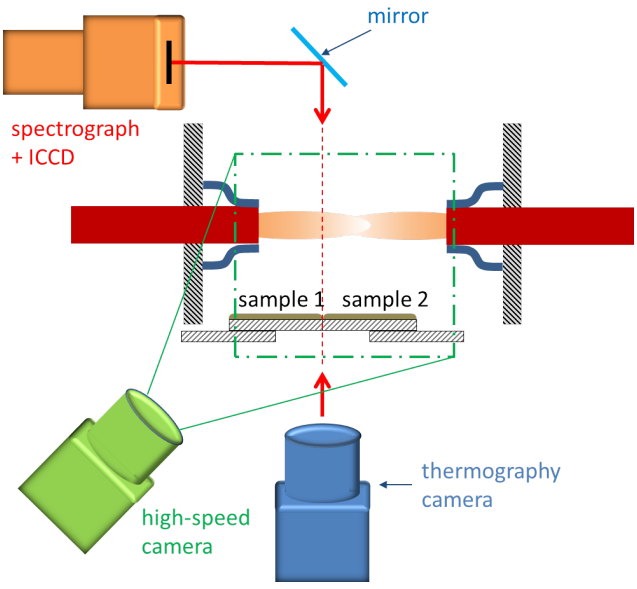


**Figure 5.** Setup of the optical diagnostics.

*Optical setup* Arc and surface erosion are observed by high speed cameras with typically 10000 fps and an acquisition time of 2 $\mu$s. (see the observation frame in Figure 5 - dash-dotted line). One camera (Motion pro Y4, black&white) has been positioned to have a front view on the

surfaces (line of sight perpendicular to arc axis and sample surface). A second camera (Motion pro Y6, color) has been used to record from the side (perpendicular to arc axis and parallel to sample surface, top view).

Optical emission spectroscopy of copper lines is used to estimate the arc temperature [7] and the radiation impact. Therefore, the arc cross section at the axial reference position is imaged to the slit of a 0.5 m spectrograph coupled with an ICCD camera. The camera is triggered at 5 ms after arc ignition with 50 $\mu$s acquisition time.

The upper surface of the coated layers as well as the backside of both samples are observed by a thermography camera with a spectral sensitivity range from about 7.5 to 12 $\mu$m and 50 fps (acquisition time of about 20 ms, 640x480 pixel array, spatial resolution 3 pixel/mm).

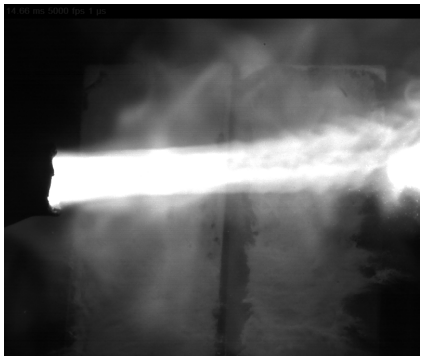

**Figure 6.** High-speed image of the arc above two samples coated with $CaCO_3$, front view.

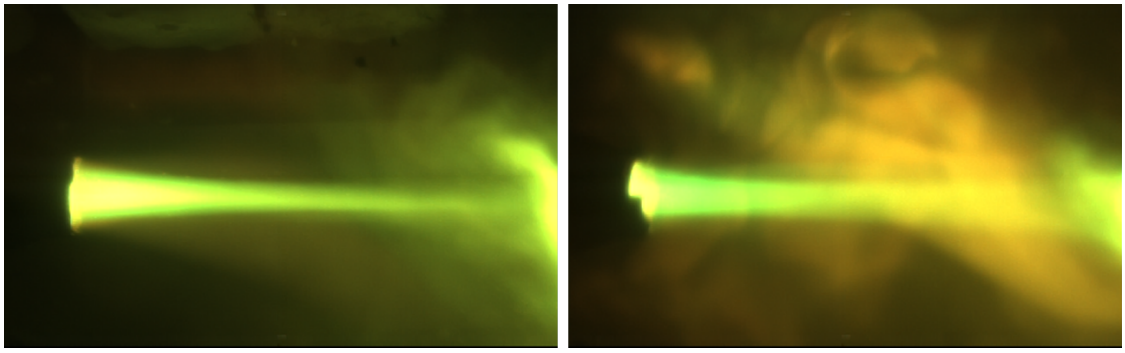

**Figure 7.** High-speed images (top view) of the arc recorded in parallel to the sample surfaces with a layer of $Mg(OH)_2$ (left side) and of $CaCO_3$ (right side).

## 3. Optical and spectroscopic analysis of the arc

The general behaviour of the arc and the arc interaction with the coated substrates has been studied by the high-speed cameras. Examples are given in the Figs. 6 and 7. Both examples are recorded at the end of the first pulse during rectangular current pulse. The cathode can be seen in each picture on the left side. The establishment of a copper vapour jet becomes clearly visible in the figures as a result of considerable copper radiation. The jet is almost stable along a distance of about 2 cm from the cathode and above sample 1. The jet becomes more irregular when interacting with a corresponding jet from the anode side over the second half of the arc length. Notice, that the jet on the cathode side is typically longer and more stable than that

from the anode side in the considered arrangement. However, because of the current course with damped amplitude, the first pulse period with the cathode jet in front of the samples causes most of the heat load on the sample surfaces.

The different interaction with layers of $Mg(OH)_2$ (left side) and of $CaCO_3$ (right side) is illustrated in Fig. 7. Whereas on the left side picture radiation from the copper vapour jet can be seen only, additional radiation occurs from vapour outside of the jet in the right picture. The observation from the movies confirms a strong evaporation of the $CaCO_3$ layer which results in the additional radiation. Spectroscopic analysis confirms that this additional radiation is not scattered light from the copper jet and includes line radiation of Ca.

A spectral range between 505 and 518 nm is considered in the emission spectroscopy of the arc in the copper vapour jet. As it has been shown in [7] this range provides a number of strong copper atomic line (Cu I) and copper ionic lines (Cu II). Currents of several kA generate typically hot arcs which are dominated by vapour from electrode erosion. Under this conditions strong line broadening can considerably hinder the application of conventional methods of plasma temperature determination from the intensity of optical thin lines (e.g. single line analysis or Boltzmann plot analysis). As an alternative method, rough estimations of the arc temperature can be obtained by comparison of the measured spectra with simple spectrum simulations. The spectral radiance resulting from Cu I and Cu II lines in the considered spectral range under the assumption of a homogeneous arc in copper vapour has been simulated for varying temperatures and pressures in a preceding work (see details in [7]).

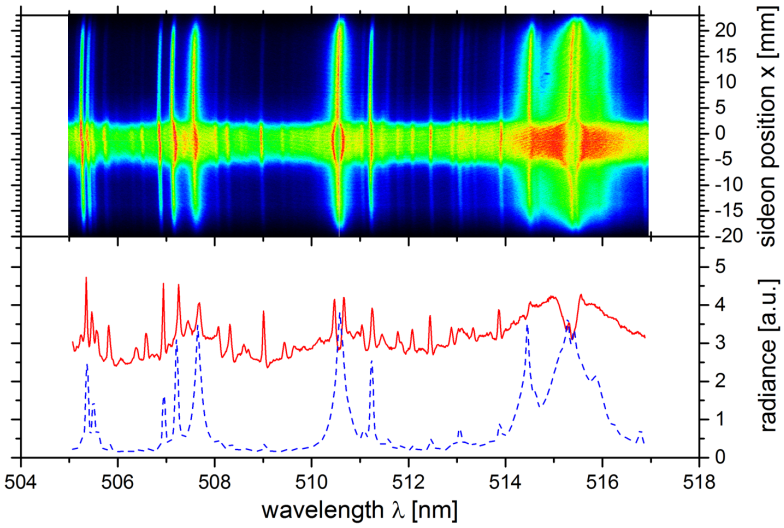


**Figure 8.** Example of the two-dimensional spectral radiance as recorded by the ICCD camera (upper part) in the middle of the first rectangular current pulse for the case of samples with $CaCO_3$ and pure plaster layers. Mean values of the spectral radiance over strips in the arc core (red solid line) and in the outer arc range (blue dashed line in the lower part).

In the present study the spectrum of the arc has been recorded at an axial position 15 mm in front of the cathode in almost all experiments. The obtained spectra are very similar and reflect the establishment of the copper vapour jet as already illustrated in the high-speed images. Exceptions occur if the region of the stagnation point between the electrode jets overlaps in the spectrum observation area. An example of the 2D image of the ICCD is shown in Fig. 8 (upper part). The signal has been averaged over a stripe covering few mm in the range of the arc core (copper vapour jet) as well as in a selected range outside the core. The resulting spectral radiances (in arbitrary units) are shown in the lower part of Fig. 8. The spectrum is dominated

by copper atomic lines as expected, in particular line groups near 515.5 nm, 510.5 nm and 507.5 nm. Copper ionic lines near to 506.5 nm, 509 nm and 512.5 nm with lower intensity can be identified. The atomic lines are strongly broadened. In the arc core the lines near 510.5 and 515.5 nm show self-absorption.

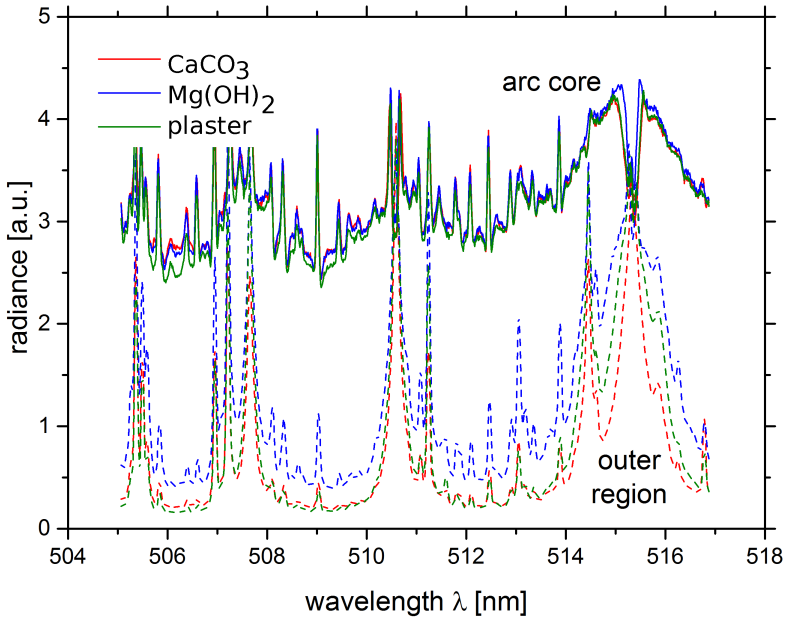


**Figure 9.** Examples of mean values of the spectral radiance over strips in the arc core (solid lines) and in the outer arc range (dashed lines) for three different cases with layers of $CaCO_3$, $Mg(OH)_2$ and pure plaster.

Mean values of the spectral radiance of the arc at peak currents in three different cases (different coatings) are compared in Fig. 9. As illustrated in the figure, the spectrum in the arc core is very similar in all experiments. There are larger differences in the spectrum outside the arc core. However, almost the same structure of lines is observed here.

The measured spectral radiances in arbitrary units have been compared with simple spectrum simulations as detailed in [7]. An example is shown in Fig. 10. The radiance measured outside the arc core shows best correspondence with simulations for a homogeneous arc of 14000 K at a copper pressure of 2 bar. Here, the intensity relation between atomic and ionic lines as well as the line width of the atomic lines have been considered in particular. The radiance measured in the arc core cannot be compared successfully with the simulations because of two reasons. Continuum radiation was not included in the simple model and may play a strong role in the arc core. Strong absorption up to self-absorption of lines cannot be simulated with the model of a homogeneous arc. However, the spectrum in the arc core seems to be dominated by these effects. Nevertheless, the intensity relation of atomic and ionic lines and its strong temperature dependence allows for conclusions about the temperature range of the arc. Because of the very low intensity of the considered CuII lines a maximum temperature between 14000 and 16000 K is estimated. The large broadening of lines indicates a large overpressure in the jet compared with atmospheric pressure.

Within the limited accuracy of the presented analysis there are no distinct differences of the arc in the first rectangular pulse in pulsed operation and at peak current in the sinusoidal operation.

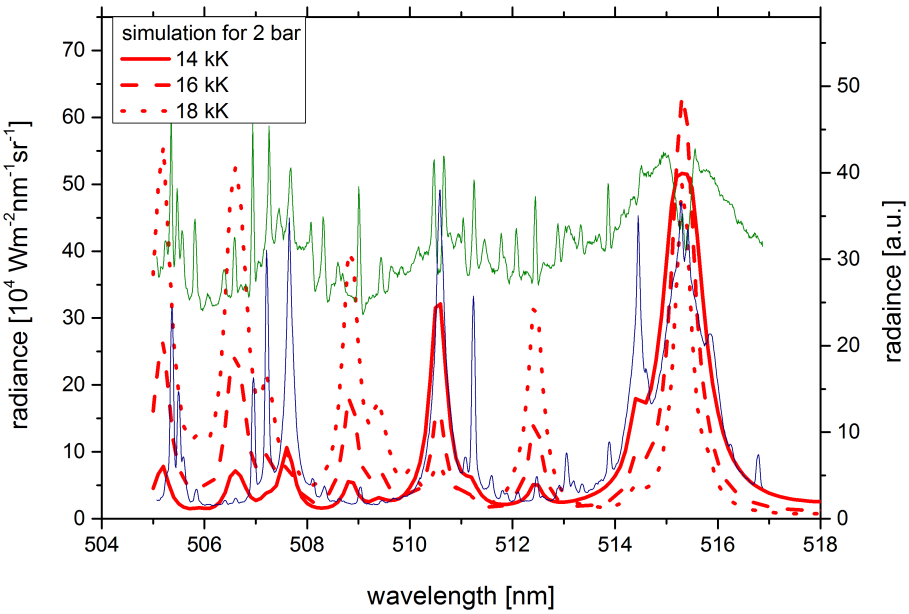


**Figure 10.** Spectral radiance from Fig, 8 (lower part) in comparison with simulated radiances from a homogeneous copper arc at 2 bar pressure and temperatures 14 to 18000 kK.

The estimation of the arc temperature and arc radius allows for estimation of the total arc radiation and of the expected heat load at the layer surfaces from the arc radiation absorption. The first rectangular current pulse over the first 5 ms is considered again as a example. The arc radius can be estimated from the typical radius of the copper jet radiation which is quite similar to the electrode radius (5 mm). Measurements of 200 V arc voltage and 4.7 kA current result in a total electric power of about 870 kW in the arc column if a cathode fall voltage of about 15 V is excluded. The net emission coefficient for pure copper for a homogeneous arc of 5 mm in radius at 15000 K is $1.2 \times 10^{10}$ $\mathrm{Wm^{-3}sr^{-1}}$ [8]. Assuming an arc of 50 mm length the total emitted radiation is about 300 kW and approximately 30% of the electric power. The part of absorbed electrical power on the surfaces of surrounding walls have been investigated for polytetrafluoroethylene nozzles in ablation dominated arcs at currents of the same order of magnitude then considered here. About 20% are reported in [6]. Considering this fraction of electric power and the distance of 25 mm from the arc axis to the sample surface in the experiments, an energy density of about 20 $\mathrm{MWm^{-2}}$ can be roughly estimated for the thermal load of the layer surfaces by plasma radiation.

## 4. Study of surface temperatures by thermography

The records of the thermography camera are illustrated by the examples in Fig. 11. The backside of coated glass substrates has been investigated in first experiments. However, because of the low heat conduction and the thickness of 3 mm of the substrates, no significant heating of the backsides could be observed.

Next measurements have been focussed on the upper surface of the layers as illustrated in the left side in Fig. 11. Records during the arc-surface interaction period could not be used because of the disturbances of remaining hot vapours. In records at about 20 to 40 ms after arcing pulse the interaction regions on the surfaces localized near to stable arc parts and with a more regular temperature development have been identified. Such regions are indicated by the red circles in Fig. 11. Mean values of the temperature in the indicated area have been recorded for each sample in steps of 20 ms.

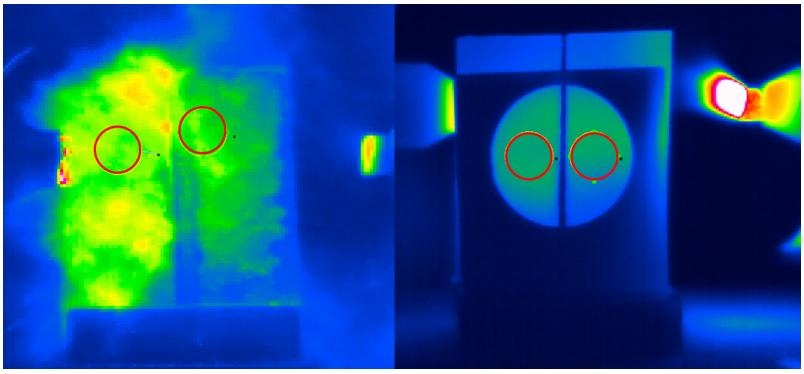

**Figure 11.** Examples of thermography camera images of the surfaces of the layers about 40 ms after arc interaction (left side) and of the backside of ceramic substrates with different layers about 4 s after arc interaction (right side). The red circles indicate the area for temperature averaging in both cases.

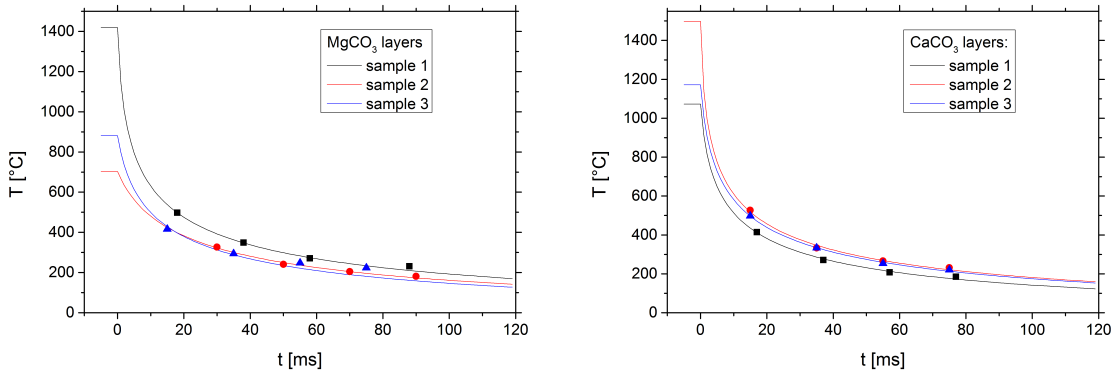


**Figure 12.** Temporal courses of the surface temperature of the layers after arc interaction for two different materials and three experiments each: symbols are measurements and lines are fit curves according to the Stefan-Boltzmann law.

The cooling of the layer surface after arc interaction should be dominated by radiation at least in the first second, and thermal conduction can be neglected. The time dependence of the surface temperature can be described by the Stefan-Boltzmann law:

$$\frac{\mathrm{d}T}{\mathrm{d}t} = A\left(T^4(t) - T_0^4\right) \tag{1}$$

where $T_0$ is the room temperature and the proportionality factor $A$ includes Stefan-Boltzmann constant, surface emissivity $\varepsilon$ as well as quantities defined by specific heat of the layer which are not known for the layer materials. The emissivities of the investigated materials have been estimated utilizing a constant temperature heat plate comparing the surface temperatures with that of a reference probe at different temperatures. The reference probe was covered with a coating of known emissivity. It revealed that the emissivity of all the investigated materials is close to one. This is reasonable for the IR spectral region of the thermography camera due to the porous and rough structure of the sample surfaces. No temperature dependence of the emissivity has been observed.

To get indications about the heating of the surfaces by the arc, the temperature measurements

have been used to find a best fit of the data with a temperature function according to eq. (1) and starting at an initial temperature $T_i$. Using $A$ and $T_i$ as fit parameters, eq. (1) has been solved numerically. Because of the low acquisition frequency of the thermography camera the delay between end of arc interaction and acquisition time has been chosen as an additional fit parameter. Examples of measurements and fitted temperature courses are shown in Fig. 12. Unfortunately, the measured values show a considerable scattering with a large overlapping between the different materials. However, significant differences in the extrapolated initial temperatures $T_i$ can be obtained. From these results it can be roughly estimated that higher initial temperatures (above 1300 K) occur in the case of $CaCO_3$ layers and lower temperatures (around 1300 K) occur at the surfaces of $MgCO_3$ and $Mg(OH)_2$ layers.

In final experiments the glass substrates have been exchanged by thin ceramic plates of 1 mm thickness. In these experiments, a significantly different heating of the backside of the substrates could be found. The low thermal conductivity of the ceramics causes a slow temperature increase at the backside surface only after arc impact. The maximum temperature is reached typically after 4 to 7 seconds. Again, samples with different layer materials and at different positions with respect to the electrodes (but in the same distance from the arc axis) have been studied. The backside surfaces of samples coated with $Mg(OH)_2$ have been heated up in average by about 20 K (scattering up to $\pm 5$ K), that with $MgCO_3$ by about 15 K whereas about 10 K difference has been obtained for $CaCO_3$ and plaster. In contrast, the backside of an uncoated ceramic sample shows a heating by 70 to 80 K. The much lower heating of the coated samples may result from the low thermal conduction in the layer and in addition from the cooling effect due to evaporation and dissociation.

## 5. Summary and outlook

The study confirms that an open setup with copper electrodes can be used to generate a free burning arc with currents in the kA range under almost stable and reproducible conditions and to study arc interaction with protective layers. Copper line radiation can be used for a rough estimation of arc temperature and the corresponding heat load on the layer surfaces. Layers made by ceramic powders can be used for an effective protection against heating and erosion of walls. However, coating techniques and the use of binders should be improved.

Next studies will focus on a more accurate analysis of the material evaporation and the heat balance of coated substrates. Furthermore, the more detailed investigation of high-current arc radiation and self-absorption effects in copper vapour is aimed.

## References

[1] Lee A, Heberlein J V R and Meyer T N 1985 High-current arc gap with ablative wall: dielectric recovery and wall-contact interaction *IEEE Trans. Components, Hybrids, and Manufacturing Technol.* **8** 129-134
[2] Seeger M, Tepper J, Christen T and Abrahamson J 2006 Experimental study on PTFE ablation in high voltage circuit-breakers *J. Phys. D: Appl. Phys.* **39** 5016-5024
[3] Rieder W, Veit Ch and Gauster E 1992 Interaction of magnetically blown break arcs with insulating walls in the contact region of interrupters *IEEE Trans. Components, Hybrids, and Manufacturing Technol.* **15** 1123-1137
[4] Doméjean E, Chévrier P, Fiévet C and Petit P 1997 Arcwall interaction modelling in a low-voltage circuit breaker *J. Phys. D: Appl. Phys.* **30** 2132-2142
[5] Rodriguez P, Didier J, Bernard G and Rowe S 1998 Arc-contact-insulating wall interactions in low voltage circuit-breakers *IEEE Trans. Power Delivery* **13** 480-488
[6] Seeger M, Niemeyer L, Christen T, Schwinne M and Dommerque R 2006 An integral arc model for ablation controlled arcs based on CFD simulations *J. Phys. D: Appl. Phys.* **39** 21802191
[7] Franke St, Methling R, Uhrlandt D, Bianchetti R, Gati R and Schwinne M 2013 Temperature determination in copper-dominated free-burning arcs *J. Phys. D: Appl. Phys.* **47** 015202
[8] Cressault Y and Gleizes A 2013 Thermal plasma properties for ArAl, ArFe and ArCu mixtures used in welding plasmas processes: I. Net emission coefficients at atmospheric pressure *J. Phys. D: Appl. Phys.* **46** 415206